Cosmic Kidney Disease: The Effects of Spaceflight and Galactic Cosmic Radiation on Renal Structure and Function

Stephen Walsh (✉ stephen.walsh@ucl.ac.uk)
University College London https://orcid.org/0000-0002-8693-1353
Keith Siew
University College London
Fatemeh Afsari
University of Florida
Maneera Al-Jaber
Anti-Doping Laboratory Qatar https://orcid.org/0000-0002-5051-7345
Noah Allen
Rensselaer Polytechnic Institute https://orcid.org/0000-0003-0998-8337
Mohammed Al-Maadheed
Anti-Doping Laboratory Qatar
Selin Altinok
The University of North Carolina at Chapel Hill
Shehbeel Arif
Children's Hospital of Philadelphia
Nourdine Bah
The Francis Crick Institute
Sergio Baranzini
University of California, San Francisco https://orcid.org/0000-0003-0067-194X
Peter Barker
University of Cambridge
Afshin Beheshti
NASA Ames Research Center
Elizabeth Blaber
Rensselaer Polytechnic Institute
Samuel Border
University of Florida
Valery Boyko
Bionetics Corp. https://orcid.org/0000-0002-3724-9294
Jessica Broni-Tabi

University College London
Keith Burling
University of Cambridge
Robert Campbell
University of Cambridge
Margareth Cheng-Campbell
Rensselaer Polytechnic Institute
Chris Cheshire
The Francis Crick Institute
Lorianna Colon
Children's Hospital of Philadelphia Research Institute
Sylvain Costes
NASA Ames Research Center https://orcid.org/0000-0002-8542-2389
Laura Cubitt
Francis Crick Institute https://orcid.org/0000-0003-1948-6795
Viola D'Ambrosio
University College London
Lovorka Degoricija
NASA Ames Research Center
Amelia Eisch
University of Pennsylvania Perelman School of Medicine
Hossein Fazelinia
Children's Hospital of Philadelphia Research Institute
Nichola Figg
University of Cambridge
Rebecca Finch
Staffordshire University
Jonathan Foox
Weill Cornell Medical College
Alison French
NASA Ames Research Center
Jonathan Galazka
NASA Ames Research Center https://orcid.org/0000-0002-4153-0249
Samrawit Gebre
NASA Ames Research Center
Peter Gordon
University College London
Alessandra Grillo
University College London https://orcid.org/0000-0001-6482-8796

Nadia Houerbi
Weill Cornell Medical College
Hossein Kahrood
Monash University
Fathi Karouia
NASA Ames Research Center https://orcid.org/0000-0002-1142-9684
Frederico Kiffer
Children's Hospital of Philadelphia https://orcid.org/0000-0001-5269-3951
JangKeun Kim
Weill Cornell Medicine https://orcid.org/0000-0002-8733-9925
Aleksandra Klosinska
University of Cambridge
Angela Kubik
Rensselaer Polytechnic Institute
Han-Chung Lee
Monash University
Yinghui Li
China Astronaut Research and Training Center https://orcid.org/0000-0002-9294-4652
Zhongwang Li
University College London
Nicholas Lucarelli
University of Florida
Steven Lynham
King's College London
Anthony Marullo
University College Cork https://orcid.org/0000-0002-1460-7167
Christopher Mason
Weill Cornell Medicine https://orcid.org/0000-0002-1850-1642
Irina Matei
Weill Medical College of Cornell University, Drukier Institue for Children's Health, Meyer Cancer Center
https://orcid.org/0000-0002-5712-8430
Cem Meydan
Weill Cornell Medicine https://orcid.org/0000-0002-0663-6216
Sayat Mimar
University of Florida
Vidya Mohamed-Ali
University College London
Masafumi Muratani
University of Tsukuba https://orcid.org/0000-0002-0276-8000

Ahmed Naglah
University of Florida
Charlotte Nelson
University of California San Francisco
Kevin Nestler
The George Washington University
Jerome Nicod
The Francis Crick Institute https://orcid.org/0000-0003-2459-3480
Kevin O'Shaughnessy
University of Cambridge https://orcid.org/0000-0002-1476-7566
Lorraine Christine De Oliveira
Federal University of São Paulo (UNIFESP)
Leah Oswalt
McAllister Heart Institute and Department of Pharmacology, The University of North Carolina at Chapel Hill, Chapel Hill, NC, USA https://orcid.org/0000-0001-7097-0801
Eliah Overbey
Weill Cornell Medicine
Vaksha Patel
University College London
Laura Ioana Patras
Weill Cornell Medical College
San-huei Polo
NASA Ames Research Center
María Rodríguez-Lopez
The Francis Crick Institute https://orcid.org/0000-0002-2066-0589
Samuel Rodriques
The Francis Crick Institute
Candice Roufosse
Imperial College London https://orcid.org/0000-0002-6490-4290
Omid Sadeghi-Alavijeh
University College London
Rebekah Sanchez-Hodge
The University of North Carolina at Chapel Hill
Lauren Sanders
NASA Ames Research Center
Anindya Sankar
University of Florida
Pinaki Sarder
University of Florida

Jonathan Schisler
The University of North Carolina at Chapel Hill, Chapel Hill https://orcid.org/0000-0001-7382-2783
Ralf Schittenhelm
Monash University https://orcid.org/0000-0001-8738-1878
Annalise Schweickart
Weill Cornell Medicine
Ryan Scott
KBR, NASA Ames Research Center https://orcid.org/0000-0003-0654-5661
Dai Shiba
Japan Aerospace Exploration Agency https://orcid.org/0000-0003-3808-5428
Terry Lim Kam Sian
Monash University https://orcid.org/0000-0001-7038-1214
Willian Silveira
Staffordshire University
Hubert Slawinski
The Francis Crick Institute https://orcid.org/0000-0002-8996-8477
Scott Smith
NASA Johnson Space Center https://orcid.org/0000-0001-9313-7900
Daniel Snell
The Francis Crick Institute
Julio Sosa
University Health Network https://orcid.org/0000-0001-5516-5724
Joel Steele
Monash University https://orcid.org/0000-0002-3070-9761
Marshall Tabetah
Purdue University https://orcid.org/0000-0002-1651-7659
Erwin Tanuwidjaya
Monash University
Akira Uruno
Tohoku University Graduate School of Medicine https://orcid.org/0000-0002-9224-0161
Michael Vaughan
Ghent University https://orcid.org/0000-0002-9979-1265
Simon Walker-Samuel
University College London https://orcid.org/0000-0003-3530-9166
Elizabeth Wan
University College London
Masayuki Yamamoto
Tohoku University Graduate School of Medicine
Xiaoping Yang

King's College London
Yasmin Yasmin
University of Cambridge
Sanghee Yun
University of Pennsylvania, Perelman School of Medicine https://orcid.org/0000-0001-7505-0836
Haijian Zhang
Monash University
Zhongquan Dai
State Key Laboratory of Space Medicine Fundamentals and Application
Jasminka Zimmermann
University College London
Sara Zwart
USRA https://orcid.org/0000-0001-8694-0180
Eduardo A.C.Almeida
NASA Ames Research Center
Chutong Zhong
University College London

Article

Keywords:

Posted Date: October 12th, 2023

DOI: https://doi.org/10.21203/rs.3.rs-2982830/v1

Additional Declarations: Yes there is potential Competing Interest. Samuel Rodriques is an active shareholder in Curio Bio, which commercializes Slide-seq.

Abstract

Missions into Deep Space are planned this decade. Yet the health consequences of exposure to microgravity and galactic cosmic radiation (GCR) over years-long missions on indispensable visceral organs such as the kidney are largely unexplored. We performed biomolecular (epigenomic, transcriptomic, proteomic, epiproteomic, metabolomic, metagenomic), clinical chemistry (electrolytes, endocrinology, biochemistry) and morphometry (histology, 3D imaging, miRNA-ISH, tissue weights) analyses using samples and datasets available from 11 spaceflight-exposed mouse and 5 human, 1 simulated microgravity rat and 4 simulated GCR-exposed mouse missions. We found that spaceflight induces: 1) renal transporter dephosphorylation which may indicate astronauts' increased risk of nephrolithiasis is in part a primary renal phenomenon rather than solely a secondary consequence of bone loss; 2) remodelling of the nephron that results in expansion of distal convoluted tubule size but loss of overall tubule density; 3) renal damage and dysfunction when exposed to a Mars roundtrip dose-equivalent of simulated GCR.

Introduction

Renewed interest in commercial and state funded space exploration has culminated in ambitious plans for 'Deep Space' missions including the Artemis Program and the Deep Space Transport/Mars Missions.

The health effects of low orbit space flight (e.g. the International Space Station) are multiple, including musculoskeletal, neurological, retinal and cardiovascular effects. The effect of space flight on visceral processes, in particular renal function, is less clear.

The kidneys are critical in regulating blood pressure, by controlling both the renin/angiotensin/aldosterone system (RAAS) and also the reabsorption of sodium chloride and water from the urine. In microgravity, the upward redistribution of blood volume with the concomitant decrease of a pressure gradient should reduce kidney perfusion. In turn, a lower perfusion pressure within the renal artery should lead to a greater release of renin and activation of the RAAS. However, studies show a marked reduction of diuresis and natriuresis in space with the RAAS, and antidiuretic hormone (ADH) increasing through unknown mechanisms[1–3]. These unexplained effects, be they mediated through known homeostatic mechanisms, or more theoretical ones, such as tensegrity[4], are germane to kidney stone formation. Astronauts have an unusually high rate of kidney stone formation, both before and after SF. This is of mission critical significance, one Soviet in-flight renal stone episode nearly caused a mission termination due to the severe symptoms, but was relieved by spontaneous stone passage by the cosmonaut just before an urgent deorbit was initiated[5]. It has been demonstrated that SF associated changes in urinary biochemistry favour kidney stone formation [6–8]. Microgravity may have a direct effect on the crystallisation and nucleation of nascent kidney stones[9], but this is dwarfed by the net biochemical urinary changes observed in SF.

The kidney is a plastic organ, and is capable of dynamically remodelling the architecture of the nephron in response to changes in blood pressure or dietary potassium. An 18 day potassium-free diet resulted in a 31% increase in rat kidney weight, which was mainly seen in the medullary collecting duct[10]. Changes in the size of nephron segments in wild type mice have been observed using advanced imaging techniques in a period as short as three days[11].

In addition to the well-studied environmental stressor of microgravity, deep space missions (that take place beyond the Van Allen belt) are exposed to space radiation. Space radiation comprises both intermittent events (e.g. Solar Particle Ejections) and constant phenomena. The most important of these from a health perspective is of Galactic Cosmic Radiation (GCR).

There is concern regarding the carcinogenic effect of GCR exposure in the panned Mars Missions. However, the kidney is an exquisitely radiation sensitive organ; it is the dose limiting organ in abdominal radiotherapy[12]. Chronic kidney dysfunction can occur with acute low linear energy transfer (LET) γ-radiation doses as low as <0.5 Gy[13], the LET dose expected on a Mars Mission. However, GCR comprises low-LET γ-radiation with protons and high energy 'HZE' ions. It has been established that exposure to HZE ions results in mitochondrial damage[14,15]. The renal proximal tubule is totally dependent on mitochondrial respiration[16] and is the tubular segment in which damage causes kidney failure[17]. Indeed, proximal tubular injury is a prominent histological feature in medical (low-LET) radiation nephropathy[18]. Due to their dependence on mitochondrial aerobic respiration, proximal tubular cells are extremely vulnerable to mitochondrial damage that we would expect from HZE exposure in addition to LET radiation damage.

We hypothesised that the biochemical urinary changes seen in SF might reflect functional and morphological changes detectable in the kidney secondary to MG, possibly due to abnormal renal perfusion.

Further, we hypothesised that GCR exposure will cause mitochondrial and therefore proximal tubular dysfunction, leading to tissue damage and renal failure, in addition to the known micro and macrovascular damage caused by GCR.

In order to explore these questions, we reanalysed existing human and rodent datasets comprising clinical chemistry and multi-omic data from NASA Genelab, NASA, JAXA and SpaceX missions. We also processed novel tissue samples from the Rodent Research 10 (RR-10) mission for novel proteomic, phosphoproteomic and 2D transcriptomic analysis as well as immunohistochemistry and optical tissue clearing and 3D imaging by confocal and light microscopy.

Results

(Figure 2: Nephrolithiasis)

We analysed urinary and plasma parameters of interest for nephrolithiasis in 66 astronauts that stayed on the International Space Station (ISS) for a period between 1 and 180 days. Values were analysed across time, including before, during and after flight. Our data showed an increased urinary excretion of parameters that are considered risk factors for nephrolithiasis (**Figure 2A**). In the figure, urinary excretion of calcium is expressed as fractional excretion (FE_{Ca}). In the absence of plasma calcium abnormalities FE_{Ca} should be <1%; in astronauts, FE_{Ca} increases significantly during flight. This urinary abnormality normalises on return on Earth. A less significant increase was seen in oxalate, phosphate, uric acid urinary excretion during space flight, all rapidly decreasing at return. Urinary citrate did not significantly change and remained within normal range. There was also a decrease in urinary volume during spaceflight and an increase in urinary osmolality (Supplementary Figure X). Urinary electrolytes (chloride, sodium and potassium) remained stable during spaceflight compared to pre-flight with the exception of magnesium that, although within the normal range, significantly increased (Supplementary Figure X). The calculated values: estimated glomerular filtration rate (eGFR), aldosterone/renin ratio, FE for urinary electrolytes and water, transtubular potassium gradient (TTKG) and the ratio of tubular maximum reabsorption of phosphate (TmP) to GFR can be found in Supplementary Figure Y. Supplementary Figure Z shows plasma values from the 66 astronauts.

These data confirm an increased excretion of calcium and phosphate in the urine that normalises on return to Earth. Other parameters change towards a pro-lithogenic profile in space (urinary excretion of oxalate and uric acid and decreased urinary volume), however, citrate, a key player in lithogenesis, was not depleted. This suggests that there might be other mechanisms underlying the increased risk of nephrolithiasis in space.

To test this hypothesis, we analysed plasma and kidney tissue multi-omic data from human and mouse samples (**Figure 2B**) for disease ontologies related to kidney stone formation. The nephrolithiasis and related ontologies were heavily represented across different datasets, providing orthogonal confirmation of real changes in the gene products comprising this ontology. In contrast, hypercalciuria and hyperoxaluria ontologies were scantily represented.

The volcano plot displaying rodent kidney tissue phosphoproteomic data (**Figure 2C**) shows a decreased phosphorylation of SLC12A1, the furosemide-sensitive Na-K-Cl cotransporter expressed in the thick ascending limb of the loop of Henle. This transporter is regulated by the calcium-sensing receptor (CaSR) and genetic (i.e. Bartter syndrome) or pharmacological (e.g. furosemide) impairment of SLC12A1 leads to hypercalciuria.

The changes in faecal microbiome between space flight and ground controls (**Figure 2D**), highlighted in red are statistically significant. Overall, these microbiota changes would be expected to confer a protective profile for nephrolithiasis, implying that the increased urinary oxalate excretion is not diet or microbiota-dependent.

Pathway analysis of novel plasma metabolomic data from humans in spaceflight (Inspiration 4, **Figure 2E**) shows a striking over-representation of Arginine biosynthesis and Arginine-Proline metabolism; Hydroxy-L-Proline is a precursor to glyoxylate[19], and acts as a substrate to produce glyoxylate in the mitochondria of renal proximal tubular cells[20].Further, Arginine-Proline metabolism has been implicated in toxic nephrolithiasis[21]. Glycerophospholipids are the main lipid component of cell membranes and pathway enrichment is compatible with remodelling events (reviewed by Han [22]). Citric Acid Cycle pathway enrichment is common to many metabolomic analyses of oxalosis; malate is a precursor to oxaloacetate and oxalate.

(Figure 3: Remodelling)

To investigate whether renal remodelling was occurring in spaceflight, we analysed Kyoto Encyclopaedia of Genes and Genomes (KEGG) pathway enrichment across 17 datasets comprising 2 human and 13 rodent spaceflight missions and 2 rodent simulated GCR experiments. The datasets were epigenomic, transcriptomic, proteomic and phosphoproteomic (**Figure 3A**). Enriched KEGG pathways that are repeatedly enriched across the datasets are compatible with remodelling events occurring in the kidney, these include focal adhesion, tight junction, gap junction, sphingolipids, actin and cell cycle pathways.

Proteomic analysis of urine from the Russian Roscosmos human spaceflight mission (**Figure 3B**) show ECM-turnover related proteins that were enriched 7 days after spaceflight compared to baseline. These include Fibronectin type 3, Apolipoprotein H (which binds to cell surface phospholipids), Alpha2-HS-Glycoprotein, the basement membrane protein Nidogen1, APP secretase (involved in intracellular protein turnover, Proactivator Polypeptide (involved in the lysosomal degradation of sphingolipids and CDH13 (calcium -dependent cell adhesion protein). Angiotensinogen is also enriched, which probably reflects RAAS activation which may be involved in ECM-turnover and putative remodelling.

3D imaging of optically cleared rodent tissue from RR-10 spaceflight mission (**Figure 3C**). The sample is stained for the canonical distal convoluted tubule (DCT) marker SLC12A3 (Blue) and the collecting duct marker AQP2 (green). Automated morphometry shows a significant change in the intensity and distribution of DCT tubule/area ratio and nuclear density between baseline and spaceflight tissue.

(Figure 4: Disease Ontology Pathways)

To understand the common processes occurring across the multiple human and rodent, SF and GCR exposed proteomic and transcriptomic datasets, we plotted enriched kidney relevant disease ontologies that were reproduced in our diverse cohort of datasets. Many of the same ontologies are represented in both the SF and simulated GCR experiments. Ontologies that are particularly enriched include amyloidosis, nephrotic syndrome and membranous glomerulonephritis, reflecting the presence of acute phase and inflammatory gene products in addition to the profibrotic and cell death gene products represented in the CKD5, renal fibrosis and renal insufficiency ontologies. The heavily enriched peripheral vascular disease and endothelial damage ontologies reflect the known endothelial and microvascular damage marker gene products enriched across the multiple GCR and SF datasets.

(Figure 5: GCR induced damage)

We then examined tissue that was only exposed to simulated GCR, in order to understand the effect of simulated GCR alone, rather than SF exposed animals, which will always have a component of GCR exposure in addition to MG, even inlow earth orbit. To do this we utilised animals that had acute exposure to GCR followed by rapid sacrifice (BNL experiments) and also acute exposure to simulated GCR and sacrifice at 6 months post exposure (NSRL-22A experiment).

Firstly, we looked for functional evidence of glomerular, proximal tubular and distal tubular function. Urinary biochemical analysis (**Figure 5A**) showed significantly greater urinary protein excretion in GCR vs sham animals, consistent with a glomerular lesion. There was no significant difference in urinary glucose, which is a highly specific, but not very sensitive marker of proximal tubular dysfunction in non-diabetic animals. Finally, there was significantly greater magnesuria in GCR exposed animals, consistent with downregulated magnesium reabsorption in the loop of Henle or the distal convoluted tubule. Next we performed fluorescence in situ hybridisation (RNAScope) to ascertain the presence and density of pathogenic miRNA species previously implicated in tissue damage in SF[23] (**Figure 5B**). Kidney tissue was algorithmically segmented into relevant regions (cortex, outer stripe of the outer medulla (OSOM), inner stripe of the outer medulla (ISOM), inner medulla (IM)) and the staining density was measured using QPath. The pathogenic mi-RNA 125A was significantly increased in the ISOM, particularly in the vascular compartment (arrows) which corresponds to the thick ascending limb of the loop of Henle, the thin descending limb of the loop and the medullary collecting duct. This mi-RNA species is implicated in vascular damage and the ISOM is also the site of the vascular bundle[24], a complex structure which is the bottleneck of all blood flow to and from the inner medulla. Further, serial tissue sections of stained kidney tissue (hematoxylin and eosin, Masson's trichrome stain) were examined by a blinded expert histopathologist. There was a thrombotic microangiopathy seen in GCR exposed tissue from two animals (**Figure 5C**).

To further understand the effect of simulated GCR on specific cell types in the kidney, we performed 2D spatial transcriptomics (Slide-seq[25]) on GCR exposed renal tissue (BNL-1 experiment). Cell types were inferred using a published renal cell atlas[26], which were mapped onto individual data points which accurately reproduced anatomy (**Figure 5D**). Transcriptional changes in specific cell types were then examined. Immunoglobulin components were heavily overexpressed by many cell sub-populations (proximal convoluted tubular cells, proximal straight tubular cells, loop of Henle and distal convoluted tubular cells), presumably reflecting increased B-cell activity in the interstitium. SGK1 transcriptional activity was decreased in PCT and PST cells. SGK1 is a master regulator of a number of epithelial membrane transporters, including canonical segment specific transporters. Heavy metal scavenging ligands, such as metallothionein-2, were transcriptionally upregulated in the PST and LoH; possibly related to local oxidative damage; with simulated GCR this may be due to metallic HZE particles.

Discussion

We have presented a large volume of data encompassing both human and rodent data, extant and novel multi-omics datasets (including epigenomic, spatial mRNA and miRNA transcriptomic, phospho/proteomic, metabolomic, metagenomic), historical and extant clinical chemistry and novel imaging data from 16 SF and 5 GCR missions to examine the effect of SF on kidney function and to try and infer the likely effect of deep space travel on renal function.

Our data supports the hypothesis that SF (likely but not exclusively due to MG) causes structural and functional renal remodelling, causing of the changes seen in the urinary biochemistry in astronauts.

These biochemical changes are known to be critical in the pathogenesis of kidney stone formation; a condition that occurs disproportionally commonly in astronauts, and that is potentially mission critical.

The increased risk for nephrolithiasis in space has been historically attributed to the negative impact of microgravity on bone mineral density that leads to increased reabsorption of bone, release of calcium salts in the bloodstream, increased renal load and therefore increased urinary excretion of calcium and phosphate. Our historical data (from 66 astronauts) confirms hypercalciuria, and the phosphoproteomic data shows decreased phosphorylation of SLC12A1, which will cause decreased paracellular reabsorption of divalent cations in the loop of Henle, and thus renal calcium and magnesium wasting.

Hyperoxaluria also occurs during spaceflight. Oxalate is freely filtered by the glomerulus and almost entirely excreted in the urine. Increased urinary oxalate reflects increased plasma oxalate load that could come from either increased endogenous liver production or increased absorption by the gut. The latter could be caused by several conditions such as increased dietary oxalate, malabsorptive conditions or altered microbiome. Dietary data were not available, and we assumed an absence of malabsorptive conditions. Spaceflight affects the gut microbiome[27], metagenomic analysis of effect of spaceflight on the microbiome showed that Oxalobacter, the bacterium primarily responsible for oxalate metabolism[28] increases during spaceflight Bacteroides, a bacterium that was found to be increased in stone formers[29], and Bifidobacterium, a pro-biotic able to metabolize oxalate in the gut[30], were enriched and depleted in spaceflight respectively. It is difficult, based on this non-quantitative data to ascribe a primary, or even secondary microbiome-related aetiology for increased stone formation in spaceflight.

Proposed interventions to prevent potential mission critical kidney stone formation in spaceflight include increasing urine output by maximising oral fluid intake[31], oral potassium citrate supplementation[32] and lithotripsy[33]. While these are sensible and may indeed be effective, none deal with the hypercalciuria that has been consistently shown in human space travellers. Thiazide diuretics reduce urinary calcium excretion[34]; (possibly by ECV contraction causing increased proximal tubular calcium reabsorption[35]) and reduce age related bone mineral density loss[36]. The pharmacological target of thiazides, SC12A3 has reduced phosphorylation in spaceflight; this predicts a likely poor effect of thiazides in reducing hypercalciuria.

Could the dephosphorylation of SLC12A1 guide us toward a therapeutic target to reduce spaceflight induced hypercalciuria? SLC12A1 activity is modulated by the calcium sensing receptor (CaSR); calcilytics (CaSR antagonists); well tolerated but disappointing in their utility for treating terrestrial osteoporosis[37], might be one potential avenue to manipulate SLC12A1 activity to ameliorate spaceflight induced hypercalciuria.

References

1. Grigoriev, A. I., Morukov, B. V. & Vorobiev, D. V. Water and electrolyte studies during long-term missions onboard the space stations SALYUT and MIR. *Clin. Investig.* **72**, 169–189 (1994).
2. Drummer, C. *et al.* Water and sodium balances and their relation to body mass changes in microgravity. *Eur. J. Clin. Invest.* **30**, 1066–1075 (2000).
3. Christensen, N. J., Drummer, C. & Norsk, P. Renal and sympathoadrenal responses in space. *Am. J. Kidney Dis.* **38**, 679–683 (2001).
4. Ingber, D. E. Tensegrity: The Architectural Basis of Cellular Mechanotransduction. *Annu. Rev. Physiol.* **59**, 575–599 (1997).
5. Pietrzyk, R. A., Jones, J. A., Sams, C. F. & Whitson, P. A. Renal Stone Formation Among Astronauts. *Aviat. Space Environ. Med.* **78**, A9–A13 (2007).
6. Gs, A., Pa, W., On, L., LKh, P. & Ct, P. [Assessment of the risk factors for urolithiasis in cosmonauts during long flights]. *Aviakosmicheskaia Ekol. Meditsina Aerosp. Environ. Med.* **30**, 24–32 (1996).
7. Whitson Peggy A., Pietrzyk Robert A., Pak Charles Y.C., & Cintron Nitza M. Alterations in Renal Stone Risk Factors after Space Flight. *J. Urol.* **150**, 803–807 (1993).
8. Whitson, P. A., Pietrzyk, R. A., Morukov, B. V. & Sams, C. F. The Risk of Renal Stone Formation during and after Long Duration Space Flight. *Nephron* **89**, 264–270 (2001).
9. Kassemi, M. & Thompson, D. Prediction of renal crystalline size distributions in space using a PBE analytic model. 1. Effect of microgravity-induced biochemical alterations. *Am. J. Physiol.-Ren. Physiol.* **311**, F520–F530 (2016).
10. Elger, M., Bankir, L. & Kriz, W. Morphometric analysis of kidney hypertrophy in rats after chronic potassium depletion. *Am. J. Physiol.-Ren. Physiol.* **262**, F656–F667 (1992).
11. Saritas, T. *et al.* Optical Clearing in the Kidney Reveals Potassium-Mediated Tubule Remodeling. *Cell Rep.* **25**, 2668-2675.e3 (2018).
12. Yang, G. Y. *et al.* Renal Atrophy Secondary to Chemoradiotherapy of Abdominal Malignancies. *Int. J. Radiat. Oncol.* **78**, 539–546 (2010).
13. Patel, Z. *Evidence Report: Risk of Cardiovascular Disease and Other Degenerative Tissue Effects from Radiation Exposure*. https://ntrs.nasa.gov/search.jsp?R=20150016006 (2015).
14. Shimura, T., Kobayashi, J., Komatsu, K. & Kunugita, N. Severe mitochondrial damage associated with low-dose radiation sensitivity in ATM- and NBS1-deficient cells. *Cell Cycle* **15**, 1099–1107 (2016).

15. Kim, H.-N. *et al.* Simulated Galactic Cosmic Rays Modify Mitochondrial Metabolism in Osteoclasts, Increase Osteoclastogenesis and Cause Trabecular Bone Loss in Mice. *Int. J. Mol. Sci.* **22**, 11711 (2021).
16. Bagnasco, S., Good, D., Balaban, R. & Burg, M. Lactate production in isolated segments of the rat nephron. *Am. J. Physiol. - Ren. Physiol.* **248**, F522–F526 (1985).
17. Chevalier, R. L. The proximal tubule is the primary target of injury and progression of kidney disease: role of the glomerulotubular junction. *Am. J. Physiol. Renal Physiol.* **311**, F145-61 (2016).
18. Cohen, E., P. Chapter 10: Radiation Nephropathy. in *Onco-Nephrology Curriculum* (2016).
19. Knight, J., Jiang, J., Assimos, D. G. & Holmes, R. P. Hydroxyproline ingestion and urinary oxalate and glycolate excretion. *Kidney Int.* **70**, 1929–1934 (2006).
20. Knight, J. & Holmes, R. P. Mitochondrial Hydroxyproline Metabolism: Implications for Primary Hyperoxaluria. *Am. J. Nephrol.* **25**, 171–175 (2005).
21. Ma, C., Kang, H., Liu, Q., Zhu, R. & Cao, Z. Insight into potential toxicity mechanisms of melamine: An in silico study. *Toxicology* **283**, 96–100 (2011).
22. Han, X. Lipidomics for studying metabolism. *Nat. Rev. Endocrinol.* **12**, 668–679 (2016).
23. Malkani, S. *et al.* Circulating miRNA Spaceflight Signature Reveals Targets for Countermeasure Development. *Cell Rep.* **33**, 108448 (2020).
24. Ren, H. *et al.* Spatial organization of the vascular bundle and the interbundle region: three-dimensional reconstruction at the inner stripe of the outer medulla in the mouse kidney. *Am. J. Physiol. Renal Physiol.* **306**, F321-326 (2014).
25. Rodriques, S. G. *et al.* Slide-seq: A scalable technology for measuring genome-wide expression at high spatial resolution. *Science* **363**, 1463–1467 (2019).
26. Clark, J. Z. *et al.* Representation and relative abundance of cell-type selective markers in whole-kidney RNA-Seq data. *Kidney Int.* **95**, 787–796 (2019).
27. Siddiqui, R., Qaisar, R., Goswami, N., Khan, N. A. & Elmoselhi, A. Effect of Microgravity Environment on Gut Microbiome and Angiogenesis. *Life* **11**, 1008 (2021).
28. Stewart, C. S., Duncan, S. H. & Cave, D. R. Oxalobacter formigenes and its role in oxalate metabolism in the human gut. *FEMS Microbiol. Lett.* **230**, 1–7 (2004).
29. Ticinesi, A. *et al.* Calcium Oxalate Nephrolithiasis and Gut Microbiota: Not just a Gut-Kidney Axis. A Nutritional Perspective. *Nutrients* **12**, 548 (2020).
30. Klimesova, K., Whittamore, J. M. & Hatch, M. Bifidobacterium animalis subsp. lactis decreases urinary oxalate excretion in a mouse model of primary hyperoxaluria. *Urolithiasis* **43**, 107–117 (2015).
31. Pa, W., Ra, P. & Cf, S. Urine volume and its effects on renal stone risk in astronauts. *Aviat. Space Environ. Med.* **72**, 368–372 (2001).
32. Whitson, P. A. *et al.* Effect of potassium citrate therapy on the risk of renal stone formation during spaceflight. *J. Urol.* **182**, 2490–2496 (2009).

33. Simon, J. C., Dunmire, B., Bailey, M. R. & Sorensen, M. D. Developing Complete Ultrasonic Management of Kidney Stones for Spaceflight. *J. Space Saf. Eng.* **3**, 50–57 (2016).
34. Nijenhuis, T. *et al.* Thiazide-induced hypocalciuria is accompanied by a decreased expression of Ca2+ transport proteins in kidney. *Kidney Int.* **64**, 555–564 (2003).
35. Nijenhuis, T. *et al.* Enhanced passive Ca2+ reabsorption and reduced Mg2+ channel abundance explains thiazide-induced hypocalciuria and hypomagnesemia. *J. Clin. Invest.* **115**, 1651–1658 (2005).
36. Bolland, M. J. *et al.* The effect of treatment with a thiazide diuretic for 4 years on bone density in normal postmenopausal women. *Osteoporos. Int.* **18**, 479–486 (2007).
37. Cipriani, C., Nemeth, E. F. & Bilezikian, J. P. Chapter 71 - Drugs acting on the calcium receptor: Calcimimetics and calcilytics. in *Principles of Bone Biology (Fourth Edition)* (eds. Bilezikian, J. P., Martin, T. J., Clemens, T. L. & Rosen, C. J.) 1657–1670 (Academic Press, 2020). doi:10.1016/B978-0-12-814841-9.00071-3.

Methods

Experimental Design and Statistics

To integrate datasets from across different omics, species, missions and tissues, all biomolecules (e.g. phosphoproteins, proteins, transcripts and methylated DNA) were linked back to their HGNC gene symbol, aggregated and collapsed to single genes (e.g.multiple phosphosites, isoforms, CpG sites) and converted to the human orthologs where necessary. To perform over-representation analysis in Metascape using the DisGeNET database, the less stringent nominal p-value of $P<0.05$ was used to threshold differentially expressed hits within each dataset for analysis (with the exception of RR-23 where the adjusted p-value was used to threshold the number of hits to a manageable number), with a $-\text{Log}_{10}$(P-value) of 2 being considered significant for ontological term enrichment.

This approach reduces the risk of false-negatives due to potentially overly stringent multiple comparison adjustment of the p-value at an individual dataset level, while mitigating the risk of false-positives at the convergence of hits during ontological term enrichment. The degree of confidence in the validity of results can then be drawn from the robustness of replication across orthogonal and/or independent datasets.

Figures

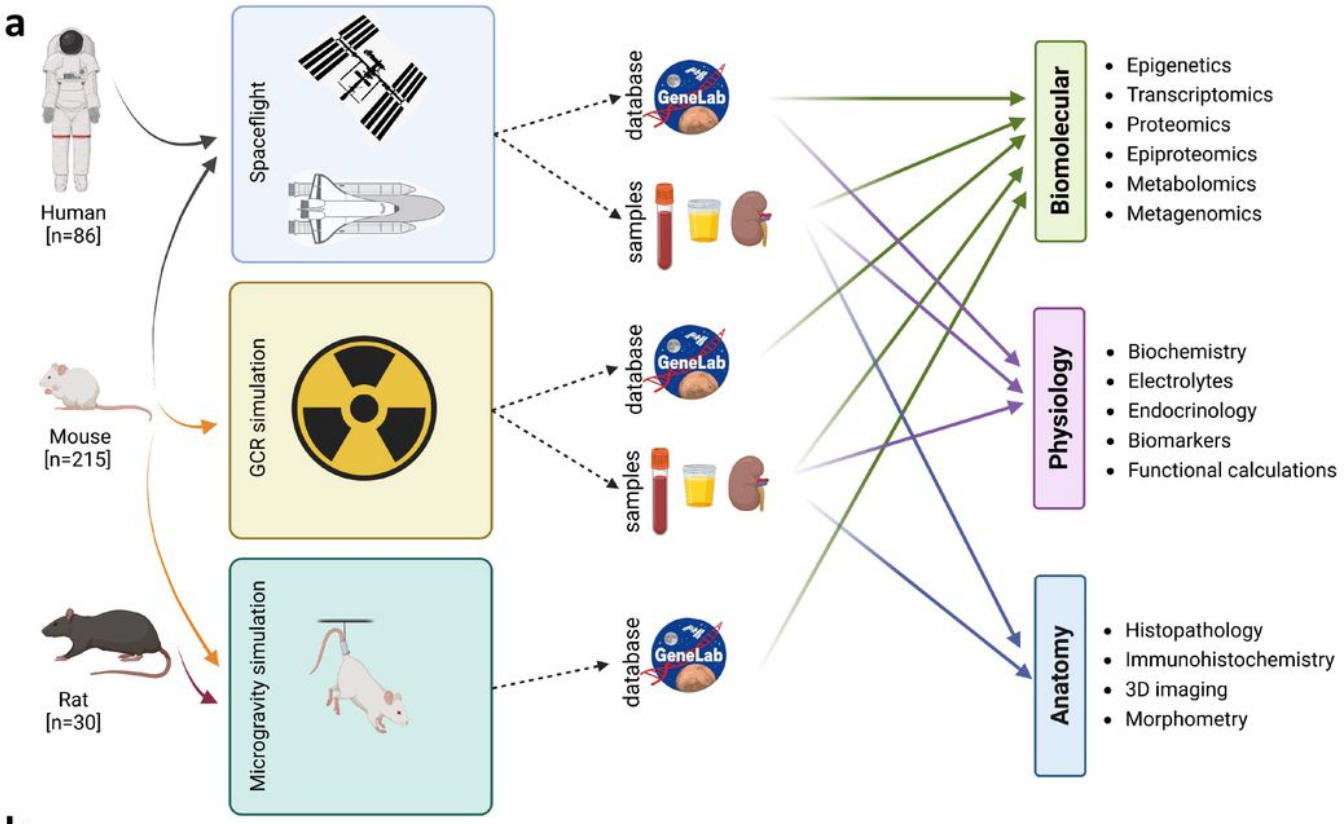

b

Mission	Experimental Condition	Species	Sex	Background	GCR (mG)	Mission Duration (d)	Sample Collection	n	Control	Data Source	Tissue	DNA Meth	RNA	Protein	PTMs	Metab	Clin Chem	Morpho	Microbes
Inspiration4	Spaceflight	Human	Mix	USA	Unknown	3	R+0	4	Paired	Original	P, U			✓		✓	✓		
JAXA	Spaceflight	Human	♂	Japan	Unknown	120	L+120	6	Paired	Original	P		✓						
NASA	Spaceflight	Human	Mix	USA	Unknown	180	L+120	66	Paired	Database	P, U						✓		
Roscosmos	Spaceflight	Human	♂	Russia	Unknown	199	R+1	10	Paired	Database	P, U			✓					
BNL-1	simGCRsim	Mouse	♀	C57BL/6	500.0	~1.5yr sim	PE+1	10	Unpaired	Original	K		✓					✓	
	MGsim				N/A	14	PE+1	10	Unpaired	Original	K							✓	
	simGCRsim + Mgsim				500.0	~1.5yr sim	PE+1	10	Unpaired	Original	K							✓	
BNL-2	simGCRsim	Mouse	♀	C57BL/6	500.0	~1.5yr sim	PE+1	10	Unpaired	Original	K							✓	
	MGsim				N/A	14	PE+1	10	Unpaired	Original	K							✓	
	simGCRsim + Mgsim				500.0	~1.5yr sim	PE+1	10	Unpaired	Original	K							✓	
BNL-3	simGCRsim	Mouse	♀	C57BL/6	500.0	~1.5yr sim	PE+1	10	Unpaired	Original	K, P, U		✓	✓				✓	
	MGsim				N/A	14	PE+1	10	Unpaired	Original	K							✓	
	simGCRsim + Mgsim				500.0	~1.5yr sim	PE+1	10	Unpaired	Original	K							✓	
NSRL-22A	GCRsim	Mouse	♀	C57BL/6	750.0	~2.5yr sim	PE+180	12	Unpaired	Original	K, P, U			✓			✓	✓	
	GCRsim	Mouse	♂	C57BL/6	750.0	~2.5yr sim	PE+180	12	Unpaired	Original	K, P, U			✓			✓	✓	
STS-135	Spaceflight	Mouse	♀	C57BL/6CR	4.7	13	R+0	7	Unpaired	Database	F								✓
RR-1	Spaceflight	Mouse	♀	C57BL/6J	5.0	38	L+38	6	Unpaired	Database	K, F	✓	✓	✓					✓
RR-3	Spaceflight	Mouse	♀	BALB/c	5.9	41	L+41	6	Unpaired	Database	K	✓	✓	✓					
RR-6	Spaceflight	Mouse	♀	C57BL/6NTac	8.2	29	R+4	9	Unpaired	Database	F								✓
					16.1	57	L+75	9	Unpaired	Database	F								✓
RR-7	Spaceflight	Mouse	♀	C3H/Hej	4.4	25	L+25	5	Unpaired	Database	K		✓						
					13.2	75	L+75	5	Unpaired	Database	K		✓						
				C57BL/6	4.4	25	L+25	5	Unpaired	Database	K		✓						
					13.2	75	L+75	5	Unpaired	Database	K		✓						
RR-9	Spaceflight	Mouse	♂	C57BL/6J	5.5	33	R+1	5	Unpaired	Database	F								✓
RR-10	Spaceflight	Mouse	♀	B6129SF2/J	4.2	28	L+28	10	Unpaired	Original	K, F		✓	✓	✓			✓	✓
RR-19	Spaceflight	Mouse	♀	C57BL/6N	5.2	35	R+0	8	Unpaired	Database	P			✓					
RR-23	Spaceflight	Mouse	♂	C57BL/6J	5.8	37	R+1	9	Unpaired	Database	K, F		✓					✓	✓
MHU-1	Spaceflight	Mouse	♂	C57BL/6J	9.0	35	R+2	6	Unpaired	Original	P		✓						
MHU-3	Spaceflight	Mouse	♂	C57BL/6NCrl	9.0	31	R+0	6	Unpaired	Database	K, P		✓			✓			
CNSA	MGsim	Rat	♂	Sprague-Dawley	N/A	28	R+0	30	Unpaired	Database	P					✓			

Figure 1

Study Design

a, Infographic representation of the study design. **b**, Details of spaceflight missions and simulations included in the project. R = return; L=launch; PE=post-exposure; P=plasma, U=urine; K=kidney; F=faecal.

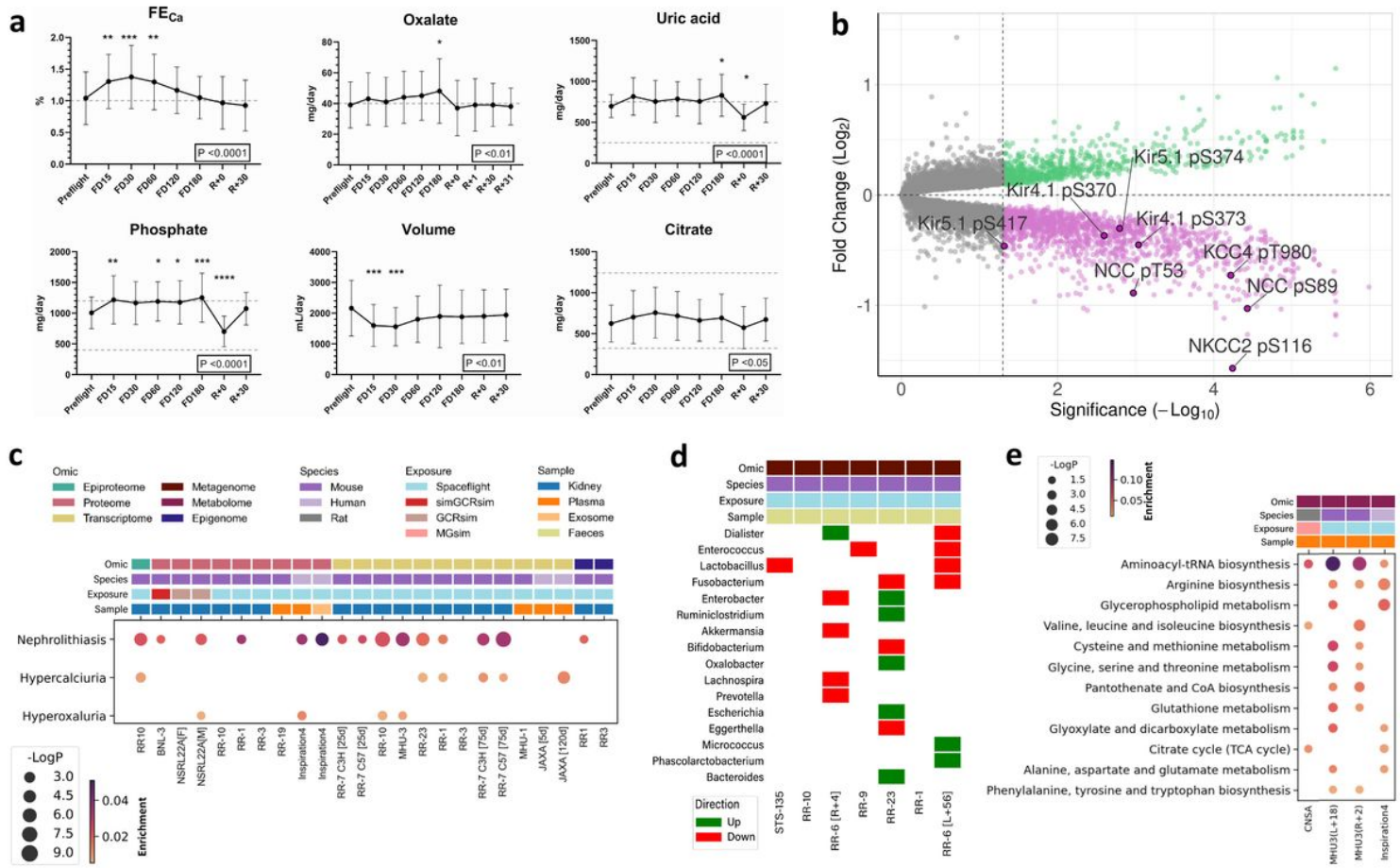

Figure 2

Contributors to nephrolithiasis risk during spaceflight

a, Urinary chemistries from NASA astronauts (n=66) exposed to spaceflight up to 180 days measured pre-flight, during (FD = flight day) and after returning (R). Dashed lines represent upper and lower normal clinical values, or upper limit where only a single line is present. Data are presented as mean ± SD. Data are presented as mean ± SD. Boxed P-values report the repeated measure one-way ANOVA result; all timepoints were compared to pre-flight by pairwise multiple comparison Bonferroni corrected *post-hoc* tests (* $p < 0.05$, ** $p < 0.01$, *** $p < 0.001$, **** $p < 0.0001$). FE_{Ca}; Fraction Excretion of Calcium. **b**, Volcano plot of differentially phosphorylated amino acid residues detected in phosphopeptide-enriched kidney protein extract from RR-10 spaceflight-exposed mice (28 days). Regulatory phosphosites in transporters and channels related to the thick ascending limb of the loop of Henle (TAL) and distal convoluted tubule (DCT) are highlighted. Green indicates a statistically significant increase in peptide phosphorylation, magenta indicates a decrease, and grey represents no significant change. A -Log_{10}(Adjusted P-value) of 1.3 was considered statistically significant (indicated by the dashed line intersecting the x-axis). Kir4.1 [KCNJ10; Kir5.1 [KCNJ16]; NKCC2 [SLC12A1]; NCC [SLC12A3]; KCC4 [SLC12A7]; pT, phosphor-threonine; pS, phosphor-serine. **c**, Multi-omic over-representation analysis of DisGeNET gene-disease associations related to nephrolithiasis. To integrate datasets from different omics modalities, species, missions and tissues, all biomolecules (e.g. phosphopeptides, proteins,

transcripts and methylated DNA) were converted to the human orthologs where necessary and linked back to their HGNC gene symbol, aggregated and collapsed to single genes (e.g. multiple phosphosites, isoforms, CpG sites). A -Log_{10}(P-value) of 2 was considered significant for ontological term enrichment. **d**, Categorical heatmap of differential abundance directionality in nephrolithiasis-related faecal microbial taxa after spaceflight. A -Log_{10}(P-value) of 1.3 was considered significant. **e**, Over-representation analysis of KEGG module metabolic pathways with replication in at least two datasets. A -Log_{10}(P-value) of 1.3 was considered significant for ontological term enrichment. **c**, **e**, Enrichment ratio; the number of differentially expressed hits in a dataset that belong to a given ontological term, normalised to the total number of statistically significant hits in the respective dataset.

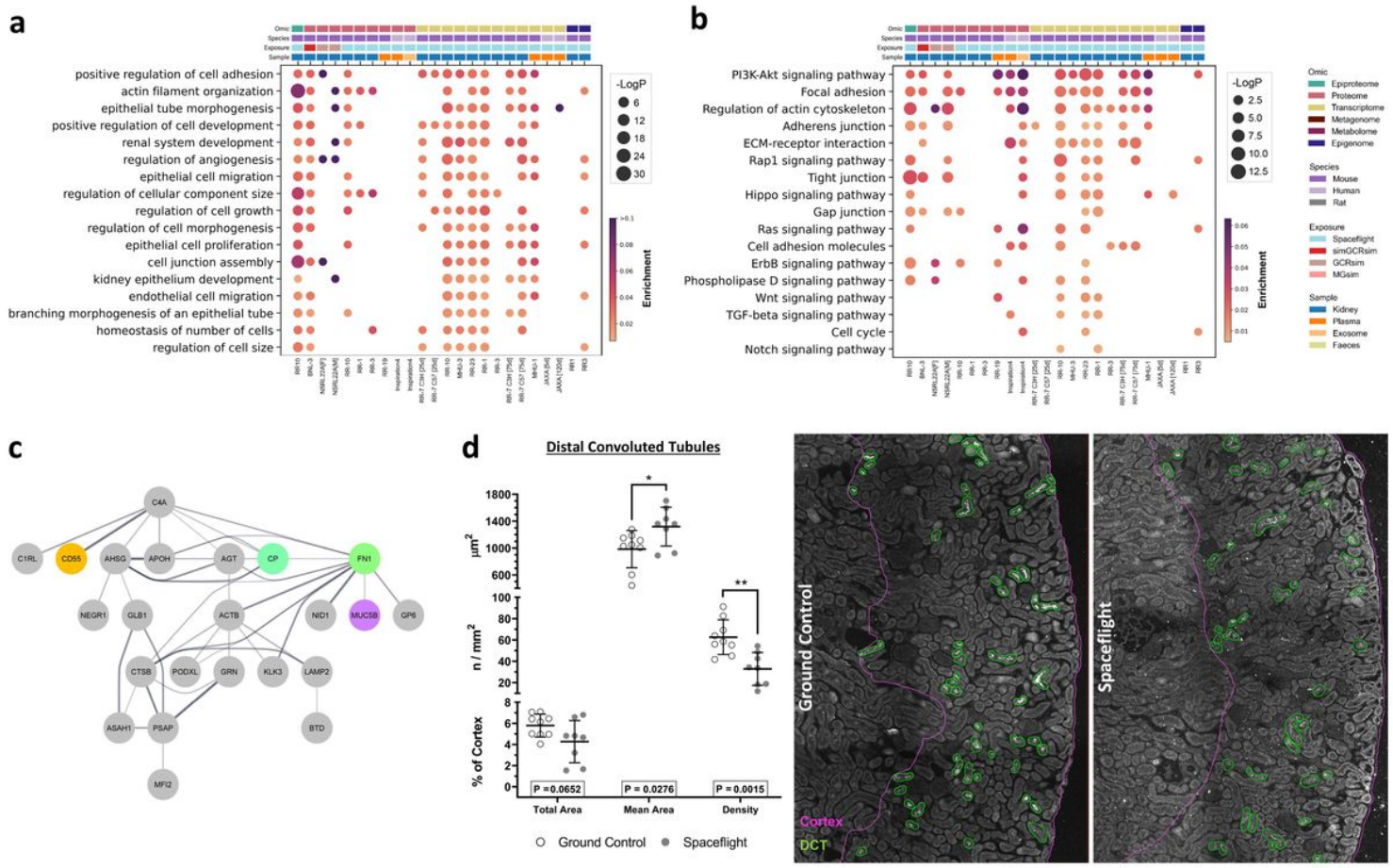

Figure 3

Spaceflight-induced nephron remodelling

a, A curated list of multi-omic over-representation analysis of GO – biological process ontological terms related to remodelling. **b**, A curated list of multi-omic over-representation analysis of KEGG pathway ontological terms related to remodelling. **a**, **b**, To integrate datasets from different omics modalities, species, missions and tissues, all biomolecules (e.g. phosphopeptides, proteins, transcripts and methylated DNA) were converted to the human orthologs where necessary and linked back to their HGNC gene symbol, aggregated and collapsed to single genes (e.g. multiple phosphosites, isoforms, CpG sites).

A -Log_{10}(P-value) of 2 was considered significant for ontological term enrichment. Enrichment ratio; the number of differentially expressed hits in a dataset that belong to a given ontological term, normalised to the total number of statistically significant hits in the respective dataset. **c**, STRING protein-protein interaction network of previously absent inflammation-associated and collagen I-associated ECM proteins that appeared in cosmonauts' urine (n=10) after 166-199 days of spaceflight exposure. **d**, Morphometric analysis of distal convoluted tubules (DCT) in RR-10 spaceflight-exposed mice (28 days) from whole slide images of kidney sections immunolabelled with NCC as a DCT marker. Representative confocal images show the annotations of DCTs and cortex region used for calculations. Data are mean ± SD. P-value of <0.05 was considered significant.

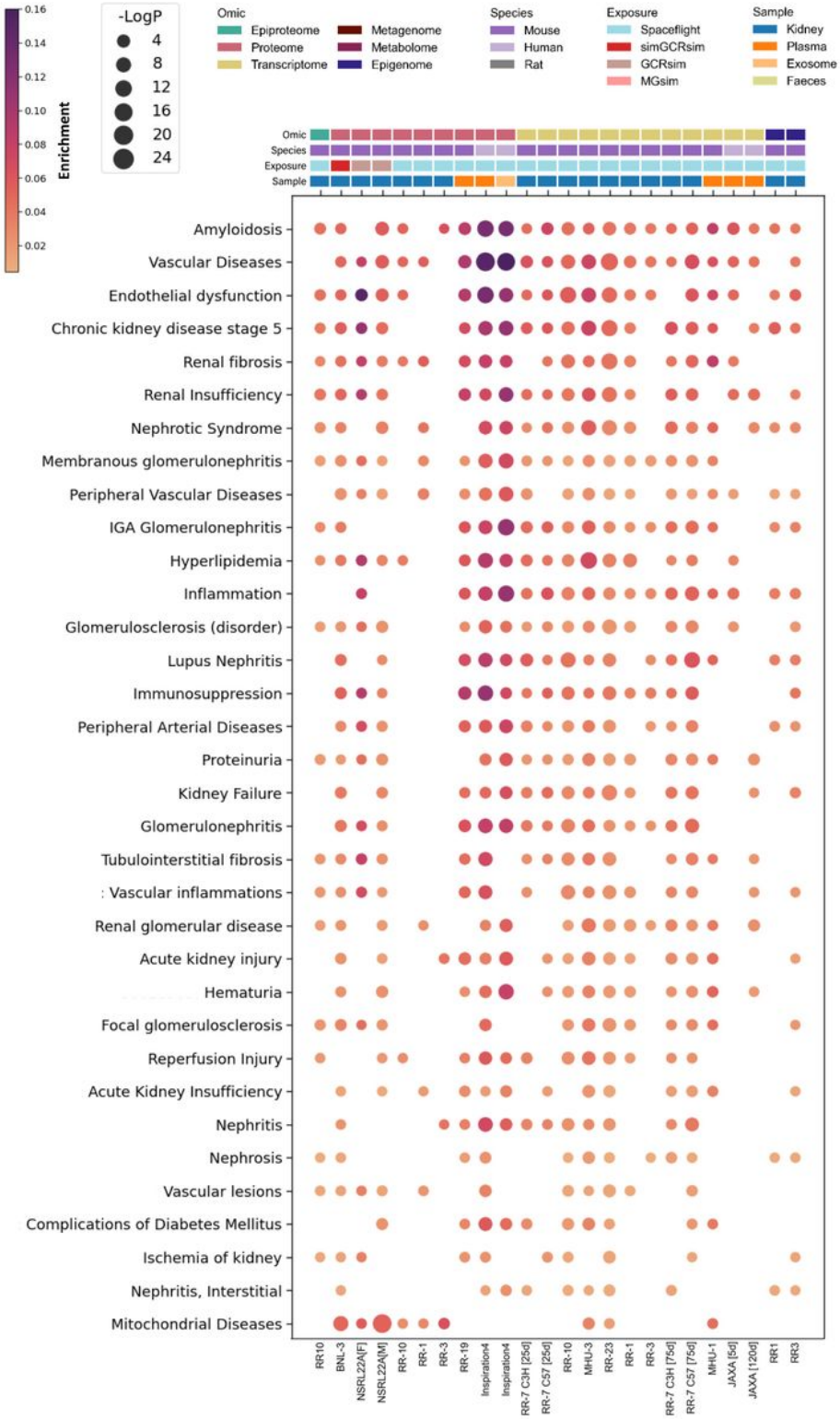

Figure 4

Multi-omic DisGeNET over-representation analysis

A curated list of enriched gene-disease associations are presented for DisGeNET ontological terms relevant to kidney health. These were ranked and represented in descending order using the following rules: 1) No. of mission datasets it replicated in; 2) most significant p-value; 3) greatest enrichment. To

integrate datasets from different omics modalities, species, missions and tissues, all biomolecules (e.g. phosphopeptides, proteins, transcripts and methylated DNA) were converted to the human orthologs where necessary and linked back to their HGNC gene symbol, aggregated and collapsed to single genes (e.g. multiple phosphosites, isoforms, CpG sites). A Log_{10}(P-value) of 2 was considered significant for ontological term enrichment. Enrichment ratio; the number of differentially expressed hits in a dataset that belong to a given ontological term, normalised to the total number of statistically significant hits in the respective dataset.

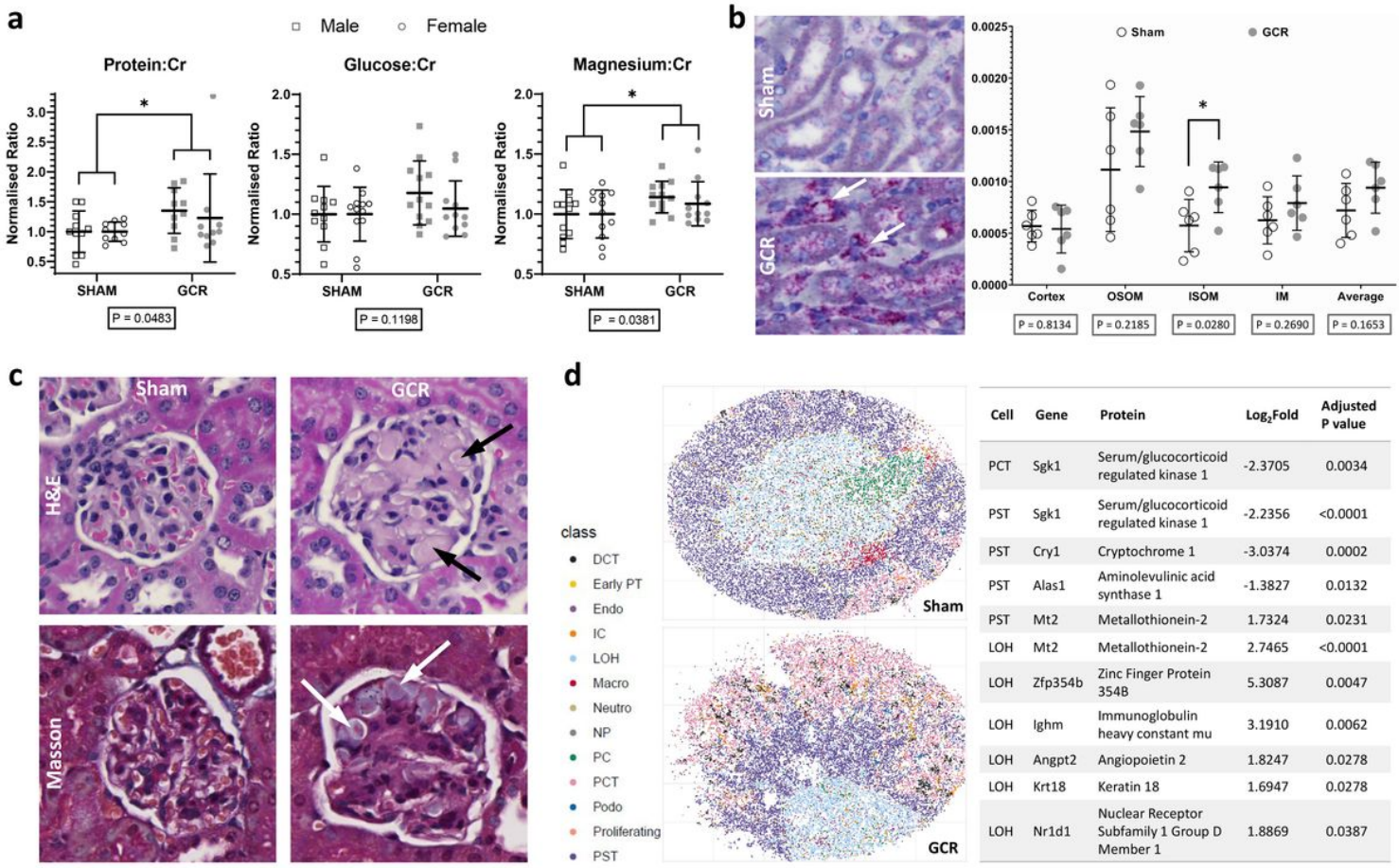

Cell	Gene	Protein	Log_2Fold	Adjusted P value
PCT	Sgk1	Serum/glucocorticoid regulated kinase 1	-2.3705	0.0034
PST	Sgk1	Serum/glucocorticoid regulated kinase 1	-2.2356	<0.0001
PST	Cry1	Cryptochrome 1	-3.0374	0.0002
PST	Alas1	Aminolevulinic acid synthase 1	-1.3827	0.0132
PST	Mt2	Metallothionein-2	1.7324	0.0231
LOH	Mt2	Metallothionein-2	2.7465	<0.0001
LOH	Zfp354b	Zinc Finger Protein 354B	5.3087	0.0047
LOH	Ighm	Immunoglobulin heavy constant mu	3.1910	0.0062
LOH	Angpt2	Angiopoietin 2	1.8247	0.0278
LOH	Krt18	Keratin 18	1.6947	0.0278
LOH	Nr1d1	Nuclear Receptor Subfamily 1 Group D Member 1	1.8869	0.0387

Figure 5

Long-term impact of galactic cosmic radiation (GCR) on kidney health.

a, Urinary chemistries from NSRL22A GCRsim-exposed mice (~2.5-year dose equivalent) expressed as creatinine ratios and then normalised to sham controls for illustrative purposes. (Cr). Boxed P-values report the two-way ANOVA treatment group factor result. Data are mean ± SD. A P-value of <0.05 was considered significant. **b**, Representative images of miR-125b staining (small red dots) in the outer medulla of haematoxylin-stained kidney sections from BNL-3 simGCRsim-exposed mice (~1.5-year dose equivalent). White arrows indicate concentrations of miR-125b staining around capillaries in the interstitium. Data are mean ± SD. A P-value of <0.05 was considered significant. OSOM; outer stripe of outer medulla. ISOM; inner stripe of outer medulla. IM; Inner medulla. Average; the simple arithmetic mean

of the four anatomical regions. **c**, Representative images of Masson's trichrome and haematoxylin & eosin (H&E) stained kidney sections from NSRL22A GCRsim-exposed mice. Arrows indicate microthrombi in the glomerular capillary tufts. **d**, Near-single cell resolution spatial transcriptomics of kidney sections from BNL-1 simGCRsim-exposed mice (~1.5-year dose equivalent). Beads are assigned identities according to their highest probable cell type classification. The table shows the differential expressed mRNA transcripts captured by different cell typed beads after exposure to GCR. An adjusted P-value of <0.05 was considered significant. DCT; distal convoluted tubule. Early PT; early proximal tubule S1. Endo; endothelial cell. IC; intercalated cell. LOH; thick ascending limb of the loop of Henle. Macro; macrophage. Neutro; neutrophil. NP; nephron progenitor cell. PC; principal cell. PCT; proximal convoluted tubule S1 + S2; Podo; podocyte. PST; proximal straight tubule S3.

Supplementary Files

This is a list of supplementary files associated with this preprint. Click to download.

- OnlineMethodstextFINALSBWKS4.docx
- 1552160supp1208177rv8dy2.xlsx
- 1552160supp1207378rv45dj.pdf
- 1552160supp1207379rv8dy2.xlsx
- 1552160supp1208131rv8dy2.xlsx
- 1552160supp1207380rv8dy2.xlsx
- 1552160supp1207381rv45dh.pdf
- 1552160supp1207382rv8dy2.xlsx
- 1552160supp1207383rv8dy2.xlsx
- 1552160supp1207384rv8dy2.xlsx
- 1552160supp1207385rv8dh3.pdf
- 1552160video1207386rv8dl5.mkv
- 1552160video1207387rv8dl5.mkv
- 1552160supp1207388rv45dv.pdf
- 1552160supp1207389rv45df.pdf
- 1552160supp1207390rv8dy3.xlsx
- 1552160supp1207391rv8dy3.xlsx
- 1552160supp1207392rv8dy3.xlsx
- 1552160supp1208178rv8d7s.docx
- flatSWalshrs.pdf